Membrane Binding and Pore Formation of the Antibacterial Peptide PGLa: Thermodynamic and Mechanistic Aspects[†]

Torsten Wieprecht,[‡] Ognjan Apostolov,[‡] Michael Beyermann,[§] and Joachim Seelig*,[‡]

Department of Biophysical Chemistry, Biocenter of the University of Basel, Klingelbergstrasse 70, CH-4056 Basel, Switzerland, and Institute of Molecular Pharmacology, Alfred-Kowalke Strasse 4, D-10315 Berlin, Germany

Received September 15, 1999; Revised Manuscript Received October 29, 1999

ABSTRACT: The antibacterial peptide PGLa exerts its activity by permeabilizing bacterial membranes whereas eukaryotic membranes are not affected. To provide insight into the selectivity and the permeabilization mechanism, the binding of PGLa to neutral and negatively charged model membranes was studied with high-sensitivity isothermal titration calorimetry (ITC), circular dichroism (CD), and solid-state deuterium nuclear magnetic resonance (^{2}H NMR). The binding of PGLa to negatively charged phosphatidylcholine (PC)/phosphatidylglycerol (PG) (3:1) vesicles was by a factor of ∼50 larger than that to neutral PC vesicles. The negatively charged membrane accumulates the cationic peptide at the lipid−water interface, thus facilitating the binding to the membrane. However, if bulk concentrations are replaced by surface concentrations, very similar binding constants are obtained for neutral and charged membranes ($K \sim 800-1500$ M^{-1}). Membrane selectivity is thus caused almost exclusively by electrostatic attraction to the membrane surface and not by hydrophobic insertion. Membrane insertion is driven by an exothermic enthalpy ($\Delta H \sim -11$ to -15 kcal/mol) but opposed by entropy. An important contribution to the binding process is the membrane-induced random coil → α-helix transition of PGLa. The peptide is random coil in solution but adopts an ∼80% α-helical conformation when bound to the membrane. Helix formation is an exothermic process, contributing ∼70% to the binding enthalpy and ∼30% to the free energy of binding. The ^{2}H NMR measurements with selectively deuterated lipids revealed small structural changes in the lipid headgroups and in the hydrocarbon interior upon peptide binding which were continuous over the whole concentration range. In contrast, isothermal titration calorimetry of PGLa solutions with PC/PG(3:1) vesicles gave rise to two processes: (i) an *exo*thermic binding of PGLa to the membrane followed by (ii) a slower *endo*thermic process. The latter is only detected at peptide-to-lipid ratios >17 mmol/mol and is paralleled by the induction of membrane leakiness. Dye efflux measurements are consistent with the critical limit derived from ITC measurements. The endothermic process is assigned to peptide pore formation and/or lipid perturbation. The enthalpy of pore formation is 9.7 kcal/mol of peptide. If the same excess enthalpy is assigned to the lipid phase, the lipid perturbation enthalpy is 180 cal/mol of lipid. The functional synergism between PGLa and magainin 2 amide could also be followed by ITC and dye release experiments and is traced back to an enhanced pore formation activity of a peptide mixture.

PGLa[1] is an antibacterial peptide of the magainin family, isolated from the skin of the African clawed frog *Xenopus laevis* (*1*−*3*). It is nonhemolytic but exhibits a broad spectrum of antimicrobial activity against Gram-positive and Gram-negative bacteria, fungi, and protozoa by enhancing the permeability of the biological membrane (*3*−*5*). The low toxicity of the magainins against eukaryotic cells makes them potential candidates for the development of new antibacterial drugs (*3*, *6*, *7*). Even though the sequence homology of PGLa with magainin 1 or 2 is low, the peptides share a number of structural features. Like magainins 1 and 2, the 21 residue peptide PGLa is positively charged (4 Lys) and adopts a random coil conformation in water (*8*, *9*). Upon membrane binding, the peptides fold into amphipathic α-helical conformations (*8*−*12*). Solid-state ^{15}N nuclear magnetic resonance (NMR) spectroscopy has shown that the PGLa helix is aligned essentially parallel to the membrane surface at low peptide-to-lipid ratios (*13*). Membrane permeabilization, however, was suggested to be induced by the formation of a peptide−lipid pore, where the PGLa helices are oriented perpendicular to the membrane surface (*14*). The selectivity of the cationic PGLa for prokaryotic systems is caused, at least partially, by a preferred interaction with negatively

[†] Supported by Swiss National Science Foundation Grant 31-42058.94.

* Corresponding author: Department of Biophysical Chemistry, Biocenter of the University of Basel, Klingelbergstrasse 70, CH-4056 Basel, Switzerland. Telephone: +41-61-267-2190. Fax: +41-61-267-2189. E-Mail: seelig1@ubaclu.unibas.ch.

[‡] Biocenter of the University of Basel.

[§] Institute of Molecular Pharmacology.

[1] Abbreviations: PGLa, *P*eptide between *G*lycine and *L*eucine *a*mide (GMASKAGAIAGKIAKVALKAL-NH_2); NMR, nuclear magnetic resonance; CD, circular dichroism; POPC, 1-palmitoyl-2-oleoyl-*sn*-glycero-3-phosphocholine; POPG, 1-palmitoyl-2-oleoyl-*sn*-glycero-3-phosphoglycerol; SUV, small unilamellar vesicle; ITC, isothermal titration calorimetry; M2a, magainin 2 amide; Tris, tris(hydroxymethyl)-aminomethane.

10.1021/bi992146k CCC: $19.00
Published on Web 12/14/1999

charged membranes (*8*, *9*). Circular dichroism (CD) experiments showed that the helicity of PGLa is larger with negatively charged vesicles than with electrically neutral vesicles (*9*). Furthermore, the thermotropic phase behavior of negatively charged phosphatidylglycerol membranes was distinctly changed upon addition of PGLa whereas that of neutral membranes was not affected (*9*). These results are relevant for biological membranes since the outer leaflet of most bacterial membranes contains indeed a high amount of negatively charged phospholipids while that of eukaryotic membranes is generally composed of neutral lipids.

PGLa acts synergistically with magainin 2 in biological systems as well as in model membranes (*5*, *10*, *15*). Possible mechanisms currently under discussion are the formation of a heteromolecular magainin 2/PGLa pore or the enhanced binding of magainin 2 due to the presence of PGLa (*14*, *15*).

Despite several functional studies on PGLa in a membrane environment, the PGLa−membrane partition equilibrium has not yet been properly characterized. Knowledge of the binding parameters for structurally different membranes and of the driving forces for membrane partitioning is essential for the understanding of the permeabilization mechanism and the membrane selectivity. We have therefore determined the thermodynamic parameters for the binding of PGLa to electrically neutral and to negatively charged lipid membranes by combining isothermal titration calorimetry (ITC) with CD spectroscopy. Structural information was obtained both on the peptide conformation (CD spectroscopy) and on the lipid structure (solid-state ^{2}H NMR spectroscopy). In addition, the extent of PGLa binding was correlated with PGLa-induced membrane permeabilization using a dye efflux assay. Finally, the synergism of PGLa and magainin 2 amide (M2a) was studied by comparing ITC binding experiments of PGLa in the presence and absence of nonlytic amounts of M2a.

MATERIALS AND METHODS

Materials. POPC and POPG were purchased from Avanti Polar Lipids. Inc., Alabaster, AL. The Fmoc amino acids for peptide synthesis were obtained from Novabiochem, Bad Soden, Germany. All other chemicals were of analytical or reagent grade. Buffer was prepared from 18 MΩ water obtained from a NANOpure A filtration system.

Peptide Synthesis. PGLa and M2a were synthesized by solid-phase methods using standard Fmoc chemistry on Tenta Gel S RAM resin (0.21 mmol/g; RAPP Polymere, Tübingen, Germany) in the continuous-flow mode on a MilliGen 9050 (Millipore, Danvers, MA) peptide synthesizer. Purification was carried out by preparative high-performance liquid chromatography (HPLC) on PolyEncap A300, 10 μm (250 × 20 mm i.d.) (Bischoff Analyzentechnik GmbH, Leonberg, Germany), to give final products >95% pure by HPLC analysis. All peptides were characterized by matrix-assisted laser desorption ionization mass spectrometry (MALDI II; Kratos, Manchester, U.K.) with the peptide content of lyophilized samples being determined by quantitative amino acid analysis (LC 3000, Biotronik-Eppendorf, Germany).

Preparation of SUVs. A defined amount of lipid in chloroform was first dried under a nitrogen stream. To remove traces of ethanol which is frequently used to stabilize chloroform, the lipid was dissolved in dichloromethane and then again dried under nitrogen and subsequently overnight under high vacuum. Typically, 2−3 mL of buffer (10 mM Tris, 100 mM NaCl, pH 7.4) was added to the lipid, and the dispersion was extensively vortexed. For preparation of small unilamellar vesicles (SUVs), the lipid dispersion was sonified (at 0 °C, in ice−water) using a titanium tip ultrasonicator until the solution became transparent. Titanium debris was removed by centrifugation (Eppendorf tabletop centrifuge, 10 min at 14 000 rpm). The lipid concentration was calculated on the basis of the weight of the dried lipid. SUVs for dye release experiments were prepared as described above using calcein-containing buffer (70 mM calcein, 10 mM Tris, pH 7.4). After sonication, the untrapped calcein was removed from vesicles by gel filtration on a Sephadex G75 column (eluent: buffer containing 10 mM Tris, 100 mM NaCl, pH 7.4). The lipid concentration was determined by quantitative phosphorus analysis (*16*).

High-Sensitivity Titration Calorimetry. Isothermal titration calorimetry was performed using a MicroCal Omega high-sensitivity titration calorimeter (Microcal, Norhampton, MA) (*17*). Solutions were degassed under vacuum prior to use. The calorimeter was calibrated electrically. The heats of dilution were determined in control experiments by injecting either peptide solution or lipid suspension into buffer. The heats of dilution were subtracted from the heats determined in the corresponding peptide−lipid binding experiments.

Circular Dichroism Measurements. CD measurements were carried out with a Jasco 720 spectrometer at wavelengths between 200 and 260 nm. Minor contributions of circular dichroism and circular differential scattering of the SUVs were eliminated by subtracting the lipid spectra of the corresponding peptide-free suspensions. The helicity of the peptides, f_h, was determined from the mean residue ellipticity, [Θ], at 222 nm according to the equation (*18*):

$$f_h = \frac{[\Theta]_{222} + 2340}{-30300} \quad (1)$$

^{2}H NMR Spectroscopy. Phosphatidylcholines, selectively deuterated in the headgroup or in the acyl chain region, were synthesized as described previously (*19*, *20*). For NMR sample preparation, a lipid film was made as described above. Defined amounts of buffer (10 mM Tris, 100 mM NaCl, pH 7.4, 1 mM EDTA, deuterium-depleted water) and peptide in buffer were added to the dried lipid (total volume: 1 mL). The mixture was intensively vortexed and subjected to 6 freeze−thaw cycles (liquid nitrogen). The lipid sample was centrifuged at 120000*g* for 120 min, and the pellet was transferred into 10 mm NMR tubes.

^{2}H NMR spectra were recorded on a BRUKER MSL 400 NMR spectrometer operating at 61.43 MHz. A quadrupole echo technique was employed with full-phase cycling by using 90° pulses of 7 μs, interpulse delays of 40 μs, recycle delays of 100−150 ms, and a spectral width of 50 kHz. A total of 2000−30 000 FIDs were accumulated depending on the content of deuterated lipid within the sample. Spectra were recorded at 28 °C

Dye Release Experiments. Aliquots of a calcein-containing SUV suspension (10−20 μL) were injected into a cuvette containing 2.5 mL of a stirred thermostated peptide solution of defined concentration (final lipid concentration was between 80 and 100 μM). Calcein release from SUVs was

determined fluorometrically by measuring the decrease in self-quenching (excitation at 490 nm, emission at 520 nm) on a Jasco FP 777 spectrofluorometer. The fluorescence intensity corresponding to 100% calcein release was determined by addition of 100 μL of 10% Triton X-100 solution.

RESULTS

Isothermal Titration Calorimetry. The enthalpy of binding of PGLa to negatively charged POPC/POPG(3:1) SUVs and electrically neutral POPC SUVs was determined from peptide-into-lipid titrations (*21*). Small aliquots of a peptide solution (5−6 μL of a 200 μM PGLa solution in buffer: 10 mM Tris, 100 mM NaCl, pH 7.4) were injected into an excess of lipid vesicles contained in the calorimeter cell (V_{cell} = 1.3353 mL, 15−25 mM lipid, same buffer) (experiment not shown). In separate control experiments, the heat of dilution was obtained by injection of peptide into buffer. Subtraction of the heat of dilution and division by the molar amount of injected peptide yielded the molar enthalpy of binding, ΔH, provided that all peptide completely binds to the membrane. In the above experiments, PGLa was completely bound to POPC/POPG(3:1) SUVs but was bound only 89% to POPC SUVs (cf. below). The enthalpy of binding, ΔH, was found to be −12.3 ± 1.4 kcal/mol at 15 °C, −12.3 ± 1.9 kcal/mol at 30 °C, and −14.6 ± 1.5 kcal/mol at 45 °C for mixed POPC/POPG(3:1) SUVs and −11.0 ± 0.6 kcal/mol for POPC SUVs at 30 °C (corrected for 100% binding).

Lipid-into-peptide titrations are required to derive binding isotherms (*21*). In this type of experiment, small aliquots of a concentrated vesicle solution (5−8 μL of 25−50 mM lipid suspensions) are injected into the calorimeter cell containing the peptide solution (between 3 and 40 μM PGLa). Calorimetric traces of typical experiments of the injection of negatively charged POPC/POPG(3:1) SUVs into PGLa solution at 30 °C are given in Figure 1. The calculation of binding isotherms is possible if the heat absorbed or released during the course of the titration arises exclusively from the binding process. In this case, a continuous decrease in the magnitude of the exothermic heat of reaction is expected with increasing injection number since less and less peptide remains free in solution (*21*). However, for the experiments shown in Figure 1, this condition is clearly not met. The exothermic binding reaction is followed by a slower endothermic reaction (see Figure 1A,C,E,G). This second reaction is already present at very low peptide concentrations [cf. Figure 1A, C^0_{PGLa} = 3 μM], and its contribution appears to increase with increasing total peptide concentration (Figure 1, peptide concentration increases from top to bottom). The endothermic process was also observed at 15 and 45 °C (data not shown). The endothermic reaction makes it impossible to derive binding isotherms for the POPC/POPG-PGLa system directly from the ITC data.

A superposition of an exothermic binding reaction with a second endothermic process was recently reported for magainin 2 amide (M2a) binding to POPC/POPG(3:1) SUVs (*22*). The endothermic process was tentatively assigned to M2a pore formation. For the latter system, pore formation occurred, however, only at peptide concentrations >7 μM, and it was thus possible to determine the binding isotherm with ITC at peptide concentrations below this limit.

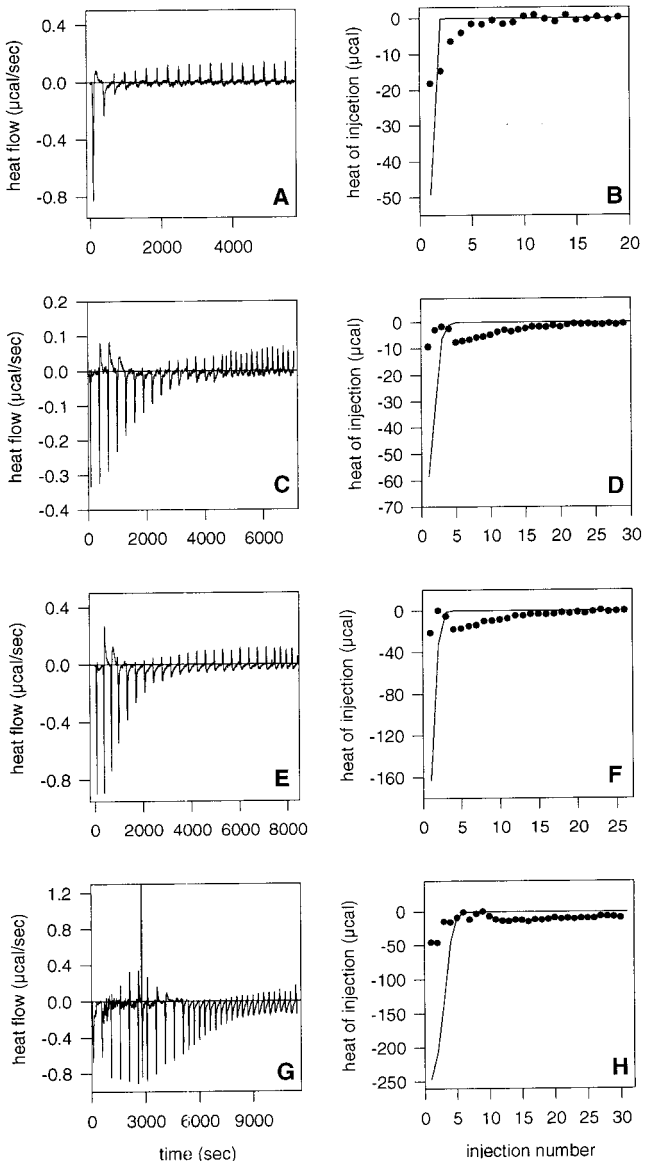

FIGURE 1: Titration calorimetry of PGLa solutions with POPC/POPG (3:1) SUVs at 30 °C (buffer: 10 mM Tris, 100 mM NaCl, pH 7.4). The panels on the left show the calorimeter tracings. The total peptide concentration increases from top to bottom. (A) Injection of 7 μL aliquots of 50 mM lipid into 3 μM PGLa. (C) Injection of 5 μL aliquots of 24.53 mM lipid into 6 μM PGLa. (E) Injection of 7 μL aliquots of 50 mM lipid into 12 μM PGLa. (G) Injection of 8 μL aliquots of 50 mM lipid into 40 μM PGLa. The panels on the right show the heat of reaction per injection vs the injection number of the experiments shown on the left. The closed circles are the experimental data. The solid lines are the calculated heats of binding based on the binding model given in the text with K = 1500 M^{-1}, ΔH = −12.3 kcal/mol, and a peptide charge z = +4.6. The simulations were performed under the assumption that all lipid was available for binding.

The interaction of PGLa with POPC/POPG(3:1) SUVs was also studied with vesicles preincubated with nonlytic concentrations of M2a. As a control, Figure 2A shows the injection of POPC/POPG (3:1) SUVs into a 6 μM PGLa solution. As in Figure 1, the reaction is characterized by an exothermic and a slower endothermic process. In Figure 2B, the titration was repeated with the modification that the POPC/POPG vesicles (24.53 mM lipid) were preincubated with 66.6 μM M2a. Preincubation of the vesicles with a small

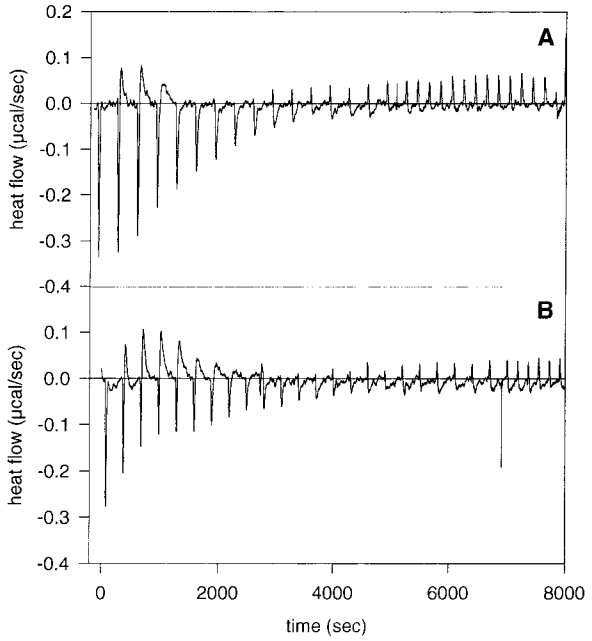

FIGURE 2: Titration calorimetry of a 6 μM PGLa solution (buffer: 10 mM Tris, 100 mM NaCl, pH 7.4) with (A) 24.53 mM POPC/POPG(3:1) SUVs and (B) 24.53 mM POPC/POPG(3:1) SUVs preincubated with 66.6 μM M2a. The figure shows the calorimeter tracings. Each peak corresponds to the injection of 5 μL of lipid suspension at 30 °C.

amount of M2a (peptide:lipid ratio 0.0027) obviously increases the contribution of the endothermic process. Control experiments in which M2a-loaded vesicles were injected into buffer revealed that the endothermic heats expected for the partial dissociation of M2a from the vesicles were negligible (not shown).

A much simpler behavior was observed for the binding of PGLa to electrically neutral POPC SUVs. Only a single exothermic process occurred (data not shown), and the binding isotherm could indeed be derived from the ITC data. Figure 3 (open circles) displays the binding isotherm at 30 °C. The extent of binding, X_b, defined as the molar amount of bound peptide per mole of total lipid, is given as a function of the free peptide concentration in solution, c_f, as derived by established procedures (*22*−*24*). For POPC membranes at low PGLa concentrations, the peptide cannot cross the bilayer, and the binding isotherm was calculated on basis of the lipid fraction present in the outer vesicle leaflet (60% of total lipid concentration, cf. below: dye release experiments).

Circular Dichroism Spectroscopy. PGLa adopts a random coil structure in buffer (spectra not shown) but folds into an α-helical conformation upon binding to a membrane. CD spectra of PGLa in the presence of POPC/POPG(3:1) SUVs at 15, 30, and 45 °C are given in Figure 4. The spectra are characterized by the helix double minimum at 208 and 222 nm. Under the condition used, the peptide is completely bound to the lipid vesicles (cf. below), and the spectra hence reflect the conformation of the vesicle-bound peptide. The helix content was calculated from the mean residue ellipticity at 222 nm and was found to decrease with increasing temperature from 84% at 15 °C to 67% at 45 °C (Table 1).

The marked spectral differences between PGLa in solution (random coil) and bound to SUVs (α-helix) allowed the determination of the binding isotherm. To this purpose, CD

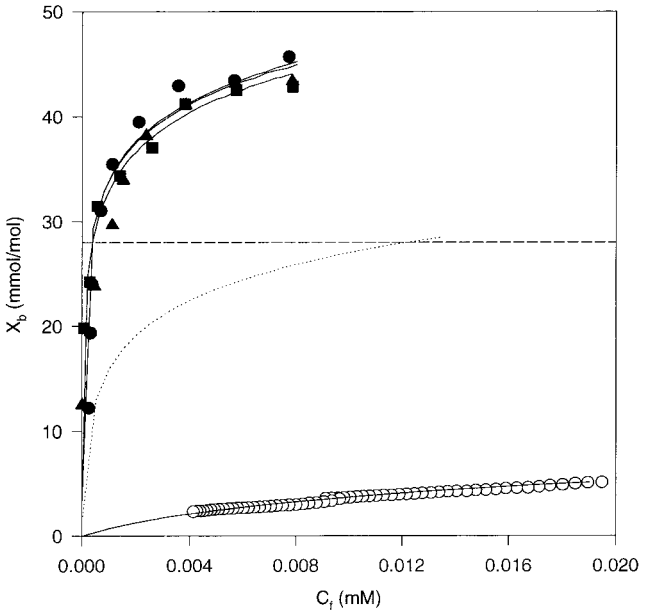

FIGURE 3: Binding isotherms for binding of PGLa to (○) POPC SUVs at 30 °C and POPC/POPG(3:1) SUVs at (■) 15 °C, (●) 30 °C, and (▲) 45 °C. The solid lines correspond to the theoretical binding isotherms calculated by combining a surface partition equilibrium with the Gouy−Chapman theory. The binding constants used for the calculation are summarized in Table 1. The dotted line corresponds to the binding isotherm of a hypothetical nonhelical PGLa (K = 38 M^{-1}, cf. text).

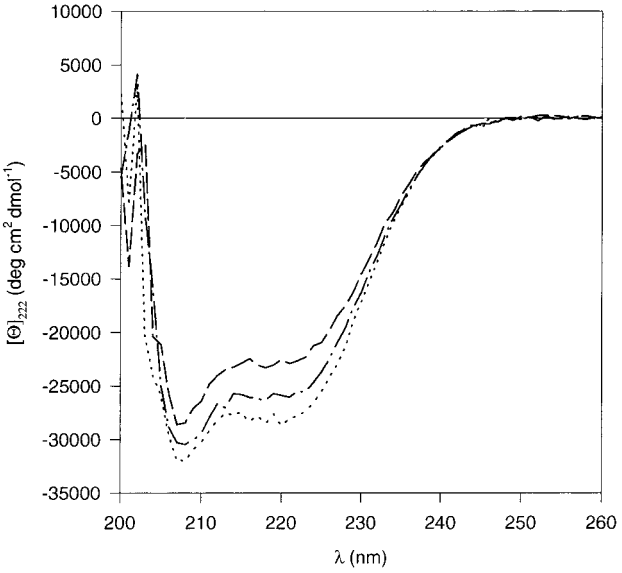

FIGURE 4: CD spectra of PGLa in the presence of POPC/POPG-(3:1) SUVs at 15 °C (dotted line), 30 °C (dashed/dotted line), and 45 °C (dashed line). The peptide concentration was 50 μM in buffer (10 mM Tris, 100 mM NaCl, pH 7.4), and the lipid concentration was 10 mM. Under these conditions, PGLa was completely bound to the membrane, and the CD spectra hence reflect the conformation of the lipid-bound peptide.

spectra of a PGLa solution (c^0_{pep} = 10 μM) were recorded in the presence of varying amounts of POPC/POPG(3:1) SUVs (lipid:peptide ratio between 0 and 300). Without lipid, the measured ellipticity reflects the conformation of the peptide in aqueous solution (Θ_W). The ellipticity decreases with increasing lipid concentration, c_L, and approaches a constant level at a lipid-to-peptide ratio of about 100. At lipid-to-protein ratios ≥100, the peptide is completely membrane-bound and characterized by the ellipticity Θ_M.

Table 1: Thermodynamic Parameters of Binding of PGLa to POPC/POPG(3:1) and POPC SUVs and Helicity of the Lipid-Bound Peptide

lipid	T (°C)	ΔH^a (kcal/mol)	K^b (M^{-1})	$\Delta G°$ [c] (kcal/mol)	ΔS^c [cal/(mol·K)]	$[\Theta]_{222}{}^d$ (deg cm^2 dmol^{-1})	helicity[e] (%)
POPC/POPG(3:1)	15	−12.3	1400	−6.5	−20.3	−27810	84
	30	−12.3	1500	−6.8	−18.1	−25500	76
	45	−14.6	1300	−7.1	−23.7	−22640	67
POPC	30	−11.0	800	−6.4	−15.0	nd	nd

[a] ΔH are directly measured binding enthalpies estimated from peptide-into-lipid titrations: 5−6 μL of 200 μM peptide solutions was typically injected into 15−25 mM POPC SUVs in buffer (10 mM Tris, 100 mM NaCl, pH 7.4). [b] Binding constants were derived using the model described in the text. [c] Free energies and entropies were calculated using the equations $\Delta G° = -RT \ln 55.5K$ and $\Delta G° = \Delta H - T\Delta S$. [d] CD experiments were performed with 10 mM POPC/POPG(3:1) SUVs and 50 μM PGLa in buffer (10 mM Tris, 100 mM NaCl, pH 7.4). Under the present conditions, all the PGLa was bound to the vesicles, and the ellipticity represents that of the bound peptide. [e] Helicity was calculated according to ref *18*; nd, not determined.

At lower lipid-to-peptide ratios, the fraction of bound peptide, $X_{P,b}$, can then be calculated as

$$X_{P,b} = (\Theta - \Theta_W)/(\Theta_M - \Theta_W) \quad (2)$$

where Θ is the measured ellipticity. The concentration of peptide remaining free in solution, c_f, is then

$$c_f = c^0{}_{pep}(1 - X_{P,b}) \quad (3)$$

The molar ratio of bound peptide per lipid, X_b, is given by

$$X_b = c_b/c_L = X_{P,b}c^0{}_{pep}/c_L \quad (4)$$

where c_L is the total lipid concentration.

A plot of X_b vs c_f yields the desired binding isotherm. The binding isotherms for binding of PGLa to POPC/POPG-(3:1) SUVs at 15, 30, and 45 °C are given in Figure 3. Under the conditions used, PGLa permeabilizes POPC/POPG(3:1) membranes (cf. the dye release experiments described below). Permeabilization was shown to be coupled with a peptide translocation from the outer to the inner leaflet of the vesicles (*14*). The binding isotherms for the mixed POPC/POPG SUVs were therefore calculated on basis of the total lipid concentration (lipid in outer layer + inner layer). Figure 3 reveals no differences in the lipid affinity of the peptides in the temperature range between 15 and 45 °C.

Binding Model and Simulation of the Isotherms. A thermodynamic analysis of the binding isotherms requires the assumption of a particular binding model. The model employed here is a *surface partition* equilibrium with the specific condition that peptide adsorption is linearly related to the peptide concentration immediately above the membrane surface (*22*−*24*) (surface concentration, c_M, and *not* to the bulk concentration, c_f):

$$X_b = Kc_M \quad (5)$$

c_M depends (i) on the free peptide concentration in bulk solution, c_f, (ii) on the peptide charge, and (iii) on the membrane surface potential. POPC/POPG(3:1) vesicles are characterized by a negative surface potential leading to an attraction of the cationic PGLa ($z \approx 4.5$ at pH 7.4; 4 Lys + partially protonated N-terminus) from bulk solution to the membrane surface. Consequently, the peptide concentration near the membrane surface (c_M) is enhanced compared to that in bulk solution (c_f). In contrast, the membrane potential of electrically neutral POPC membranes is zero. However, after binding of the first PGLa molecules to the membrane, the membrane becomes positively charged, resulting in a repulsion of further peptide from the membrane surface and hence $c_M < c_f$. Therefore, the concentration of peptide near the membrane surface differs from that in bulk solution both for negatively charged POPC/POPG(3:1) vesicles and for neutral POPC vesicles.

Using the Gouy−Chapman theory (for reviews, see refs *25*−*27*), it is possible to calculate c_M for each data point of the binding isotherm (Figure 3) and to determine the binding constant K. A detailed description of this binding model as applied to magainin peptides can be found in references *22* and *24*. The solid lines in Figure 3 are the best theoretical fits to the experimental data, and the corresponding binding constants are listed in Table 1. Interestingly, while the apparent binding constant of PGLa (expressed by the ratio of X_b to c_f for a specific c_f) is by a factor of ∼50 higher at negatively charged POPC/POPG(3:1) SUVs (K_{app} = 34 000 M^{-1} at $c_f = 1$ μM) than at POPC SUVs (K_{app} = 700 M^{-1} at $c_f = 1$ μM), the partition constants, describing the peptide transfer from the *membrane surface* into the membrane, are rather similar ($K_{POPC/POPG(3:1)}$ = 1500 M^{-1}; K_{POPC} = 800 M^{-1}).

The free energy of binding, $\Delta G°$, can be calculated according to

$$\Delta G° = -RT \ln 55.5K \quad (6)$$

where the factor 55.5 is the molar concentration of water and corrects for the cratic contribution. $\Delta G°$ corresponds to the transition of the peptide from the lipid−water interface (peptide concentration c_M) into the bilayer and was found to be between −6.4 and −7.1 kcal/mol (Table 1). Next, the entropy of binding can be calculated according to

$$\Delta S = (\Delta H - \Delta G°)/T \quad (7)$$

The entropy of binding was negative for POPC/POPG(3:1) and POPC vesicles [between −15.0 and −23.7 cal/(mol·K)], hence opposing binding of the peptide to the membrane (Table 1).

Deuterium NMR Spectroscopy. While CD spectroscopy provides detailed information about the changes in peptide structure upon membrane binding, ^{2}H NMR is the method of choice to look at peptide-induced changes in the bilayer structure (*28*). The influence of PGLa on the conformation of the phosphatidylcholine headgroup in negatively charged POPC/POPG(3:1) coarse liposomes was studied using POPC selectively deuterated in the α (CH_2 group adjacent to the phosphate) and β (CH_2 group adjacent to the nitrogen) positions of the choline headgroup. The ^{2}H NMR spectra

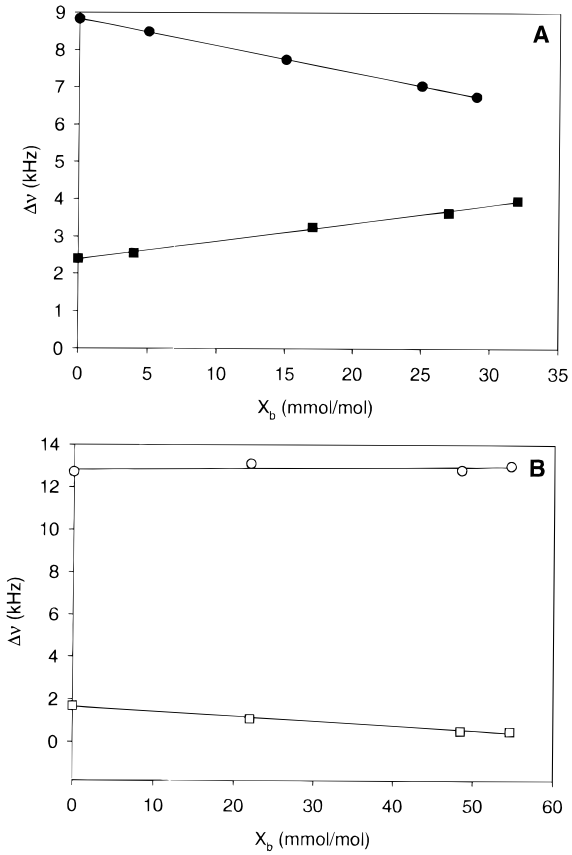

FIGURE 5: ^{2}H NMR measurements with selectively labeled phospholipids. (A) PGLa-induced conformational change of the phosphocholine headgroup in membranes composed of POPC/POPG(3:1). POPC was deuterated at the α-segment (●) and at the β-segment (■) of the choline group. (B) Influence of PGLa on the hydrocarbon region of phosphatidylcholine in POPC/POPG(3:1) membranes. POPC was deuterated in positions 9 (○) and 10 (□) at the cis-double bond of the oleic acyl chain. The figures show the variation of the quadrupole splittings with the ratio of *bound* peptide per lipid, X_b.

(not shown) were characterized by a single quadrupole splitting at all peptide:lipid ratios investigated, indicating the existence of a single time-averaged headgroup conformation. Figure 5A shows the influence of PGLa on the quadrupole splittings of the α- and β-deuterons. While the α-quadrupole splitting decreases linearly with the molar ratio of bound peptide per lipid (X_b), the β-splitting was found to increase. Linear regression of the quadrupole splitting changes yields

$$\Delta\nu_\alpha(\text{kHz}) = 8.8 - 72.4X_b\ (\text{kHz}) \quad (8)$$

$$\Delta\nu_\beta(\text{kHz}) = 2.4 + 48.4X_b\ (\text{kHz}) \quad (9)$$

The peptide effect is more pronounced for the α- than for the β-quadrupole splitting, and the ratio of the slopes is $m_\beta/m_\alpha = -0.67$. This counter-directional change of the two quadrupole splittings has been observed previously for other systems and can be explained by a charge-induced tilting of the $^-$P−N$^+$ dipole of the choline headgroup with the N$^+$ end moving away from the membrane surface (*29*, *30*).

The influence of PGLa on the hydrocarbon region of POPC/POPG(3:1) membranes was studied using POPC selectively deuterated at the double bond of the oleic acyl chain ([9′,10′-^{2}H$_2$]POPC, Figure 5B). Without PGLa, the splittings of the D-9 and D-10 deuterons were 12.7 and 1.7 kHz, respectively. Addition of PGLa decreased the D-10 splitting but hardly affected the D-9 splitting. Linear regression of the D-10 quadrupole splitting changes yields

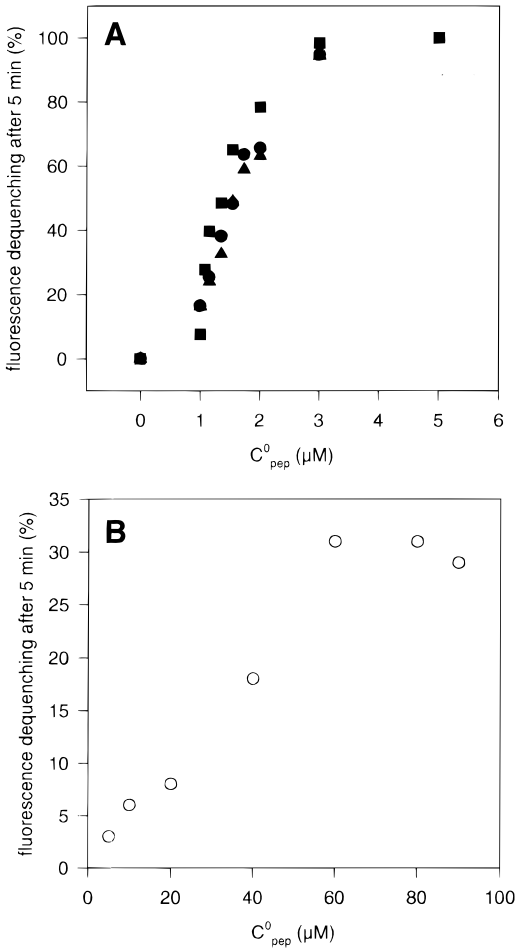

FIGURE 6: Extent of calcein leakage as a function of total peptide concentration. (A) POPC/POPG(3:1) SUVs at (■) 15 °C, (●) 30 °C, and (▲) 45 °C; (B) POPC SUVs at 30 °C. Leakage is given as the percentage of fluorescence dequenching after 5 min. The lipid concentration was (A) 87 μM and (B) 100 μM.

$$\Delta\nu_{\text{D-10}}\ (\text{kHz}) = 1.7 - 22.4X_b \quad (10)$$

A decrease of only one quadrupole splitting can be explained by a peptide-induced change of the orientation of the cis double bond rather than by an increase in the segmental fluctuations (*19*).

PGLa-Induced Membrane Permeabilization. Calcein release experiments from POPC/POPG(3:1) SUVs as well as POPC SUVs have been performed in order to correlate PGLa−membrane binding with membrane permeabilization. The addition of dye-containing SUVs to a PGLa solution induced a dye release, reflected in a fluorescence increase. Figure 6A shows the extent of fluorescence dequenching, measured 5 min after mixing of PGLa with POPC/POPG-(3:1) SUVs (Figure 6A, at 15, 30, and 45 °C) and with POPC SUVs (Figure 6B, at 30 °C), as a function of the total peptide concentration. The data reveal two interesting results: (i) An increase in temperature from 15 to 45 °C does not affect the extent of permeabilization of POPC/POPG(3:1) SUVs. The peptide concentration necessary to induce 50% dye release (EC_{50}) is always between 1.3 and 1.5 μM. (ii) The dye release from electrically neutral POPC SUVs is consid-

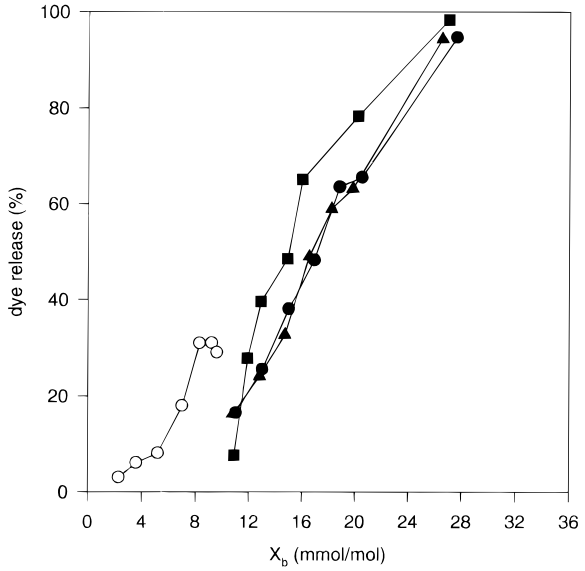

FIGURE 7: Relationship between calcein leakage and the molar ratio of *bound* PGLa per lipid, X_b, as calculated by combining the binding isotherms with the results of the dye release experiments. The symbols are as follows: release from POPC/POPG(3:1) SUVs at (■) 15 °C, (●) 30 °C, and (▲) 45 °C and release from POPC SUVs at (○) 30 °C.

erably reduced compared to negatively charged POPC/POPG(3:1) SUVs (cf. $EC_{25}^{POPC/POPG} = 1$ μM and $EC_{25}^{POPC} = 50$ μM).

The differential dye release activity of PGLa shown in Figure 6 could be caused by differences in the membrane affinity or in the ability of the bound peptide to permeabilize the membranes. To assess the potential of the *bound* peptide to enhance the membrane permeability, the dye efflux was correlated in Figure 7 with the mole fraction of *bound* peptide, X_b. The figure demonstrates that for a given amount of *bound* peptide, PGLa is even more efficient in permeabilizing POPC membranes than mixed POPC/POPG membranes.

Dye release experiments were also performed to study the functional synergism between PGLa and M2a. As previously reported for a variety of other model membrane systems (*5*, *14*, *15*), a 1:1 mixture of PGLa and M2a shows a higher activity in permeabilizing POPC/POPG(3:1) SUVs than either of the peptides alone (Figure 8A). Under the present condition, the EC_{50} value of dye release (concentration of peptide causing 50% fluorescence dequenching 5 min after addition of lipid) is 0.6 μM for M2a/PGLa (1:1), 1.6 μM for PGLa, and 2.5 μM for M2a. In analogy to the ITC experiments, we have compared the ability of PGLa to induce dye release from POPC/POPG(3:1) SUVs and from POPC/POPG(3:1) SUVs preincubated with M2a (Figure 8B). Addition of 1 μM PGLa to 81 μM POPC/POPG(3:1) led to a moderate increase of the fluorescence from a value of 1500 au to 2000 au after 5 min (~14% dequenching, trace 1 in Figure 8B). However, after preincubation of SUVs with nonlytic concentrations of M2a, the same PGLa concentration enhanced the fluorescence to 4700 au (0.1 μM M2a; M2a:lipid ratio 0.0012, 86% dequenching, trace 3 in Figure 8B) and 5000 au (0.2 μM M2a; M2a:lipid ratio 0.0024, 95% dequenching, trace 4 in Figure 8B), respectively, revealing a significantly enhanced permeabilization activity. For comparison, even a PGLa concentration of 1.2 μM caused

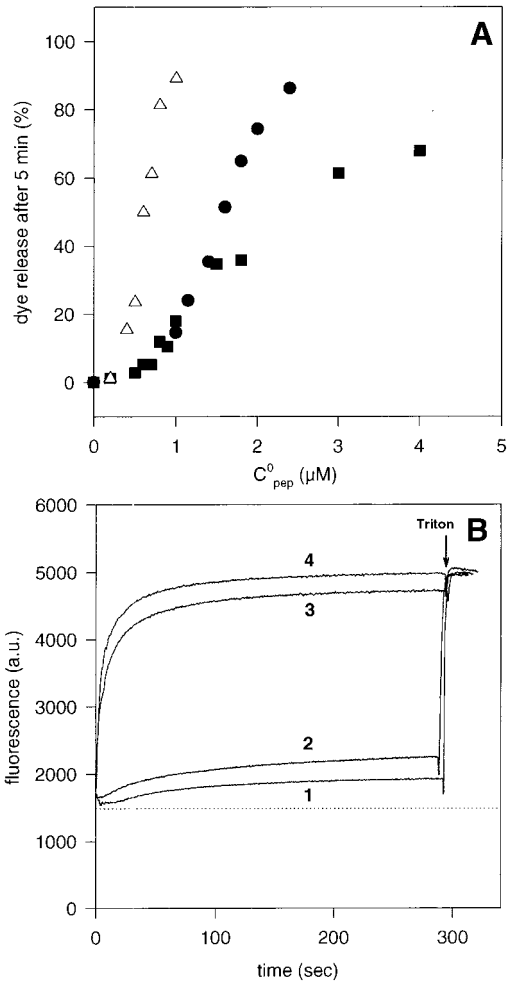

FIGURE 8: Functional synergism between PGLa and M2a. (A) Dependence of calcein leakage from POPC/POPG(3:1) SUVs at 30 °C on the total peptide concentration: (●) PGLa; (■) M2a; and (△) PGLa:M2a 1:1. The lipid concentration was 81 μM. (B) Calcein fluorescence as a function of time. The specific conditions were the following: trace 1, 81 μM POPC/POPG(3:1) SUVs + 1 μM PGLa; trace 2, 81 μM POPC/POPG(3:1) SUVs + 1.2 μM PGLa; trace 3, 81 μM POPC/POPG(3:1) SUVs preincubated with 0.1 μM M2a + 1 μM PGLa; trace 4, 81 μM POPC/POPG(3:1) SUVs preincubated with 0.2 μM M2a + 1 μM PGLa. The fluorescence value corresponding to 100% dye release was determined after addition of 100 μL of a 10% Triton X-100 solution. The dotted line corresponds to the fluorescence of the lipid suspension without addition of peptide. Preincubation of SUVs with M2a did not cause any dye release.

only about 20% fluorescence dequenching (trace 2 in Figure 8B).

DISCUSSION

Driving Forces of Membrane Binding. Transfer of PGLa from an aqueous solution into a membrane consists essentially of three steps. First, the peptide is transported from the bulk aqueous solution to the membrane surface. This step is mainly modulated by the membrane surface potential. A negative surface potential as found with POPC/POPG(3:1) vesicles results in an attraction of the positively charged PGLa to the membrane surface, while a positive surface potential (POPC + bound PGLa) repels the peptide. The second step is an incorporation of the hydrophobic peptide side chains into the hydrophobic membrane core. This step is strongly coupled to the third step, the conformational transition from a random coil to an α-helical conformation.

The model employed for the binding of PGLa to membranes is a surface partition equilibrium which corrects for the electrostatic attraction/repulsion of the peptide to/from the membrane surface (step 1) (*23*). The thermodynamic parameters listed in Table 1 reflect only steps 2 and 3, i.e., the transfer of the peptide from the membrane surface (peptide concentration c_M) to the membrane binding sites and the coil → α-helix transition. The corrected thermodynamic parameters are similar for negatively charged POPC/POPG(3:1) SUVs and electrically neutral POPC SUVs. The free energy of binding is −6.4 kcal/mol for POPC SUVs (30 °C) and −6.5 to −7.1 kcal/mol for POPC/POPG(3:1) SUVs (15−45 °C). For both membrane systems, peptide binding is driven by a negative enthalpy of −11.0 to −14.6 kcal/mol and is opposed by a negative entropy of −15.0 to −23.7 cal/(mol·K) (Table 1). The so-called selectivity of PGLa for negatively charged POPC/POPG(3:1) SUVs is thus caused essentially by electrostatic attraction, i.e., an enhanced accumulation of the peptide in the membrane vicinity. However, for a given *surface* concentration, c_M, PGLa shows almost the same free energy ($\Delta G°$) to penetrate into charged and uncharged membranes.

The binding isotherms of PGLa for POPC/POPG(3:1) SUVs could be described for X_b values up to 45 mmol/mol using the surface partitioning model. This model assumes that the PGLa remains monomeric in the lipid-bound state. A further association to peptide aggregates after binding should lead to deviations from the calculated binding isotherm, which were not observed.

The thermodynamic binding parameters of PGLa are of the same order as those found for magainin binding to negatively charged POPC/POPG(3:1) and zwitterionic POPC membranes (*22*, *24*). Since the sequence homology between M2a and PGLa is low, it can be concluded that membrane binding of antibacterial peptides depends less on the actual amino acid composition but rather on global structural properties such as peptide charge, hydrophobicity, and amphipathicity.

Three forces must be considered which drive amphipathic peptides into lipid vesicles: the hydrophobic effect, the coil−helix transition, and the nonclassical hydrophobic effect (*24*, *31*). The hydrophobic effect, i.e., the release of water molecules from the hydrophobic side chains upon membrane incorporation, is essentially an *entropy-driven* process at room temperature (*32*). Although probably contributing to the overall negative free energy of PGLa binding, the hydrophobic effect does not dominate the binding parameters as can be concluded from the large *negative* binding entropy observed in the present experiments.

Membrane binding of PGLa is energetically facilitated by a simultaneous random coil → α-helix transition (*24*, *33*). Helix formation of magainin analogues was found to entail an enthalpy change of −0.7 kcal/mol per residue and to contribute −0.14 kcal/mol per residue to the total free energy of binding (*33*). It is illustrative to apply these numbers to PGLa binding to POPC/POPG(3:1) SUVs. The helicity of PGLa is 0% in buffer, but 76% in the membrane-bound state at 30 °C. The contribution of helix formation to the binding enthalpy is hence −11 kcal/mol [−0.7 kcal/mol × 0.76 (helicity) × 21 (residues)] and accounts for ∼90% of the measured enthalpy of binding (ΔH = −12.3 kcal/mol). At 45 °C, the helix content is reduced to 67%, and helix formation contributes −10 kcal/mol (∼68%) to the binding enthalpy (ΔH = −14.6 kcal/mol). The contribution of helix formation to the *free energy* of binding is −2.2 kcal/mol at 30 °C [−0.14 kcal/mol × 0.76 (helicity) × 21 (residues)], which is 32% of the total free energy. It can be concluded that helix formation dominates the binding enthalpy and is a strong driving force for PGLa−membrane binding.

The role of helix formation in the binding of PGLa can be further illustrated by assuming a hypothetical, nonhelical peptide and calculating its binding isotherm. The free energy of binding is given by $\Delta G_{total} - \Delta G_{helix} = -4.6$ kcal/mol. The binding constant is calculated to be $K = 38\ M^{-1}$ using eq 6, and the corresponding binding isotherm is given in Figure 3 by the dotted line. The reduced membrane affinity would have drastic consequences for the membrane-permeabilizing effect. Total dye release within 5 min was reached at a ratio of bound peptide per lipid, X_b, of ∼28 mmol/mol for POPC/POPG(3:1) SUVs (cf. Figure 7), corresponding to a free peptide concentration of ∼1 μM. Assuming the same X_b value to be valid for the hypothetically nonhelical peptide, the corresponding free peptide concentration would be ∼12 μM (Figure 3, free peptide concentration, where the dotted binding isotherm crosses the line X_b = 28 mmol/mol). Therefore, the random coil → α-helix transition increases the activity of the peptide by at least 1 order of magnitude.

Membrane partitioning of amphiphilic organic molecules and small cyclic peptides, which do not undergo a conformational transition, has been found to be accompanied by an exothermic heat of reaction. This effect contradicts the traditional view that the transfer enthalpy of hydrophobic substances from the aqueous phase into a hydrophobic phase should be close to zero at room temperature (*34*, *35*). The "nonclassical" hydrophobic effect has been explained by increased van der Waals interactions between lipids or between solute and lipids upon membrane incorporation (*31*, *36*). In the case of PGLa binding to SUVs, the contribution of the nonclassical hydrophobic effect to the overall binding enthalpy is estimated to be between −1 and −5 kcal/mol ($\Delta H_{total} - \Delta H_{helix}$). This is clearly smaller than the values reported for M2a binding to POPC SUVs (between −5 and −10 kcal/mol) (*24*). It should be noted that the hydrophobic core of the PGLa helix consists mainly of alanine residues, whereas that of M2a is composed of residues with longer side chains. The latter could make more efficient van der Waals contacts and thus increase the contribution of the nonclassical hydrophobic effect to the enthalpy of binding.

Influence of PGLa on Membrane Structure. The location of PGLa within the POPC/POPG(3:1) membrane was analyzed with solid-state ^2H NMR spectroscopy of specifically deuterated lipids. First, the influence of PGLa on the α- and β-quadrupole splittings of the choline headgroup was studied (Figure 5A). Addition of PGLa to the membrane had opposite effects on the α- and β-splittings: the α-splitting decreased and the β-splitting increased. This finding can be explained by a charge-induced rotation of the $^-P-N^+$ dipole of the choline headgroup. As shown by neutron diffraction and NMR studies, the $^-P-N^+$ dipole is oriented approximately parallel to the membrane surface in neutral bilayers (*37*, *38*). In negatively charged membranes, however, the positively charged nitrogen is attracted by the membrane surface, leading to a rotation of the N-end of the dipole toward the membrane surface (*29*). Binding of the positively

charged PGLa reduces the negative membrane charge, leading to a reverse movement of the $^{+}$N-end back toward the aqueous phase. A similar behavior was observed for many other positively charged compounds, such as metal ions, organic molecules, and peptides, which bind to the membrane surface (*29*, *39*). The efficacy of the membrane-bound compounds to change the orientation of the $^{-}$P−N^{+} dipole is reflected in the slopes, m_i (see eqs 8 and 9). The slopes m_i observed for PGLa binding to POPC/POPG(3:1) vesicles ($m_\alpha = -72.4$; $m_\beta = 48.4$) are comparable to those found for melittin [$m_\alpha = -93.3$; $m_\beta = 44.4$ for POPC; (*40*)] and M2a ($m_\alpha = -67.8$; $m_\beta = 56.0$; T. Wieprecht and J. Seelig, unpublished result).

The insertion of PGLa into the hydrophobic membrane region of POPC/POPG(3:1) membranes was studied using POPC deuterated at the cis-double bond of the oleic acyl chain. PGLa decreased the D-10 splitting but had almost no effect on the D-9 splitting (Figure 5B). In the unperturbed POPC membrane, the cis-double bond is not exactly parallel to the bilayer normal but is tilted about 8° away from this axis (*19*). In the present experiments, a more random movement (increased fluctuations) would decrease both quadrupole splittings simultaneously, which is not observed experimentally. Instead, only the C-10 splitting is changed while the C-9 splitting remains virtually constant. This result can only be explained by a small change in the tilt angle of the cis-double bond.

The ^{2}H NMR results are consistent with an orientation of the PGLa helix parallel to the membrane surface as derived recently with ^{15}N solid-state NMR of oriented membranes (*13*). A parallel orientation allows the positively charged Lys side chains to remain in contact with the bilayer surface and to change the headgroup conformation. At the same time, the hydrophobic amino acids are in contact with the membrane hydrophobic core. The intercalation of PGLa between the headgroups spaces the lipids apart, and the distortion of lipid packing is sensed by a change in the tilt angle of the cis-double bond.

The NMR investigations were performed at X_b values as high as 55 mmol/mol (acyl chains) and 32 mmol/mol (headgroups) and hence under conditions where the membrane was highly permeable (cf. Figure 7). Nevertheless, the NMR data reveal a homogeneous perturbation of the lipid membrane, increasing linearly with the extent of peptide. They do not provide evidence for a phase change of the bilayer structure or any other irregularity which could be linked to peptide−peptide association or the onset of pore formation.

Pore Formation. The mechanism currently under discussion for membrane permeabilization of magainin and PGLa involves the formation of short-lived toroidal pores composed of peptides and lipids (*14*). It was shown that PGLa-induced membrane permeabilization is coupled to peptide translocation from the outer to the inner membrane leaflet and to lipid flip-flop (*14*). However, direct evidence for the existence of a pore with a well-defined structure does not exist to date. In the following, the term "pore formation" will hence be used solely to indicate the existence of an active peptide−lipid structural state leading to an enhanced membrane permeability.

We have used calcein release experiments in order to study PGLa-induced pore formation. PGLa was highly active in permeabilizing POPC/POPG(3:1) SUVs, and the extent of permeabilization was almost independent of temperature between 15 and 45 °C (Figure 6A). For electrically neutral POPC SUVs, membrane permeabilization was drastically reduced (Figure 6B). However, a plot of dye efflux vs X_b, the ratio of *bound* peptide per lipid, is more revealing. Figure 7 shows that for a given amount of bound peptide, PGLa is more efficient in permeabilizing POPC vesicles than negatively charged POPC/POPG(3:1) vesicles. An identical result was recently reported for a magainin analogue and for an amphipathic model peptide (*41*, *42*). This finding together with the thermodynamic analysis sheds light on the mechanism of peptide selectivity for negatively charged membranes: The high activity of PGLa in permeabilizing negatively charged membranes (Figure 6A vs 6B) is essentially a consequence of the accumulation of cationic peptide near the negatively charged membrane surface. Membrane selectivity is caused neither by an enhanced transfer of the peptide from the membrane surface into the membrane (compare Table 1, thermodynamic binding parameters) nor by an enhanced pore formation activity of the bound PGLa (Figure 7). Since the membrane charge in the outer leaflet of prokaryotic membranes is one of the major differences to eukaryotic membranes, we suggest that electrostatic accumulation accounts to a large extent for the prokaryotic specificity of PGLa.

The pore formation activity can also be used to understand the ITC experiments displayed in Figure 1. The lipid-into-peptide titrations with POPC/POPG(3:1) SUVs were performed under conditions of dye release, at least during the first few lipid injections (e.g., $C^0_{pep} = 3$ μM: $X_b = 11.3$ mmol/mol after first injection ≈ 20% release; $C^0_{pep} = 6$ μM: $X_b = 39$ mmol/mol after first injection ≈ 100% release; cf. Figures 3 and 7). Inspection of Figure 1 reveals an exothermic binding process and, superimposed, a second, endothermic process. Using the binding data obtained with CD spectroscopy and the binding enthalpies (Table 1), it was possible to calculate the titration curves for peptide binding proper and to compare them with the experimental results (Figure 1B,D,F,H). During the first few injections, the measured heat is considerably *less* exothermic than expected. However, in the second part of the experiments, the experimental heats are *more* exothermic than predicted. In fact, the endothermic excess enthalpy during the first injections is fully or partially recovered in consecutive injections. In analogy to the ITC data obtained for the magainin−POPC/POPG(3:1) system (*22*), we assign these deviations to a pore formation ⇔ pore disintegration process. In the initial phase of the experiment, the peptide-to-lipid ratio is high, and PGLa binding to the membrane is followed by pore formation/lipid perturbation. This is an endothermic process, and its enthalpy can be calculated from the excess enthalpy and the amount of bound peptide as 9.7 ± 1.9 kcal/mol of peptide (mean ± SD of 9 independent titration experiments with c^0_{pep} between 3 and 40 μM). For M2a, the corresponding value was found previously to be 6.2 ± 1.6 kcal/mol of peptide (*22*). For both peptides, pore formation is thus driven by entropy.

Pore formation/lipid perturbation is observed at high peptide-to-lipid ratios only. As more and more lipid is added, a critical threshold is reached below which the process of pore formation is reversed. The critical limit is given in Figure 1 by the intersection of the theoretical binding

isotherm with the experimental data as $X_b^{crit} = 18 \pm 5$ mmol/mol (9 experiments). Hence, the membrane permeability should be markedly enhanced if more than ~18 peptide molecules are bound per 1000 lipid molecules. This value, obtained from ITC experiments, is in accordance with the results of the dye efflux experiments: 50% dye release after 5 min was observed at $X_b \approx 17$ mmol/mol (see Figure 7).

At the critical limit, the lipid-to-peptide ratio is $1/X_b^{crit} \approx 56$. If the pore formation/lipid perturbation is referred to the amount of lipid involved, the enthalpy change is 180 cal/mol of lipid. This is a rather small enthalpy change compared to the gel-to-liquid-crystal transition of pure POPC ($\Delta H_{melt} \sim 8$ kcal/mol) or the bilayer−hexagonal phase transition of lipids ($\Delta H \geq 0.5$ kcal/mol). It is, however, consistent with the ^{2}H NMR spectra which indicate rather subtle changes in the lipid structure.

As the lipid concentration increases beyond the threshold value, the heat absorbed for pore formation during the first part of the experiment is released again. For the experiments shown in Figure 1, the excess heats consumed in the first part of the experiment and released in the second parts amount to 7.8/−8.1 kcal/mol (Figure 1B: $c^0_{pep} = 3$ μM), 10.2/−8.9 kcal/mol (Figure 1D: $c^0_{pep} = 6$ μM), 10.6/−8.6 kcal/mol (Figure 1F: $c^0_{pep} = 12$ μM), and 9.3/−4.1 kcal/mol (Figure 1H: $c^0_{pep} = 40$ μM). The excess enthalpy is only partially returned for peptide concentrations above 20 μM, presumably caused by a partial irreversibility of the pore formation process at high peptide concentrations.

The pore formation concept also provides insight into the lipid-into-peptide titration curves observed for PGLa after preincubation of the vesicles with small amounts of M2a. Figure 2 shows that preincubation of lipid with M2a leads to an enhanced contribution of the endothermic process to the heat of reaction during the first part of the titration. M2a and PGLa have been shown to act synergistically in biological membranes as well as in model membrane systems (*5*, *10*, *15*). In accordance with previous results, our efflux experiments revealed that a 1:1 mixture of PGLa and M2a has a higher potential to permeabilize POPC/POPG(3:1) SUVs than each of the peptides alone (*5*, *14*). Likewise, the potential of PGLa to permeabilize membranes was drastically enhanced after preincubation of the vesicles with nonlytic amounts of M2a. The dye release experiments shown in Figure 8B were done using similar peptide:lipid ratios as employed for the ITC experiments shown in Figure 2. Obviously, an enhanced endothermic excess enthalpy is accompanied by an increased membrane permeabilization. We therefore suggest that the synergism between M2a and PGLa is based on an enhanced pore formation capability of a M2a−PGLa mixture compared to the pure peptides. This is in accordance with the results recently reported by Matsuzaki et al. (*14*) that the rate of pore formation is enhanced for a pore formed by a 1:1 mixture of PGLa and M2a.

Concluding Remarks. Isothermal titration calorimetry in combination with spectroscopic techniques has been used to study the PGLa−membrane binding equilibrium and pore formation. Binding of PGLa to electrically neutral and negatively charged membranes could be described by a surface partition equilibrium after a proper correction for electrostatic effects by means of the Gouy−Chapman theory. The selectivity of PGLa for negatively charged membranes is caused by the electrostatic attraction of the highly charged peptide ($z \sim +4.6$) to the membrane surface and not by hydrophobic forces. No differences were found in the hydrophobic insertion energies of PGLa between neutral and negatively charged membranes. ^{2}H NMR spectroscopy revealed subtle changes in the lipid structure which varied smoothly with the peptide concentration, even under conditions where titration calorimetry and permeability measurements indicated the formation of membrane-active pores. Hence, only a minor fraction of the peptide can be involved in pore formation. Alternatively, membrane permeability could be induced by a lipid perturbation mechanism. Membrane-active pore formation/perturbation requires a critical peptide-to-lipid limit of ~18 peptides per 1000 lipids (or less than ~55 lipids per peptide) and is an endothermic, entropy-driven process. 1:1 mixtures of PGLa and magainin 2 amide enhance the permeability synergistically. The functional interplay of the two compounds is reflected in the thermodynamic data by an enhanced endothermic pore formation.

REFERENCES

1. Hoffmann, W., Richter, K., and Kreil, G. (1983) *EMBO J. 2*, 711−714.
2. Andreu, D., Aschauer, H., Kreil, G., and Merrifield, R. B. (1985) *Eur. J. Biochem. 149*, 531−535.
3. Soravia, E., Martini, G., and Zasloff, M. (1988) *FEBS Lett. 228*, 337−340.
4. Westerhoff, H. V., Juretic, D., Hendler, R. W., and Zasloff, M. (1989) *Proc. Natl. Acad. Sci. U.S.A. 86*, 6597−6601.
5. Gomes, A. V., de Waal, A., Berden, J. A., and Westerhoff, H. V. (1993) *Biochemistry 32*, 5365−5372.
6. Zasloff, M. (1987) *Proc. Natl. Acad. Sci. U.S.A. 84*, 5449−5453.
7. Maloy, W. L., and Kari, U. P. (1995) *Biopolymers 37*, 105−122.
8. Jackson, M., Mantsch, H. H., and Spencer, J. H. (1992) *Biochemistry 31*, 7289−7293.
9. Latal, A., Degovics, G., Epand, R. F., Epand, R. M., and Lohner, K. (1997) *Eur. J. Biochem. 248*, 938−946.
10. Williams, R. W., Starman, R., Taylor, K. M., Gable, K., Beeler, T., Zasloff, M., and Covell, D. (1990) *Biochemistry 29*, 4490−4496.
11. Matsuzaki, K., Harada, M., Funakoshi, S., Fujii, N., and Miyajima, K. (1991) *Biochim. Biophys. Acta 1063*, 162−170.
12. Wieprecht, T., Dathe, M., Schümann, M., Krause, E., Beyermann, M., and Bienert, M. (1996) *Biochemistry 35*, 10844−10853.
13. Bechinger, B., Zasloff, M., and Opella, S. J. (1998) *Biophys. J. 74*, 981−987.
14. Matsuzaki, K., Mitani, Y., Akada, K. Y., Murase, O., Yoneyama, S., Zasloff, M., and Miyajima, K. (1998) *Biochemistry 37*, 15144−15153.
15. Westerhoff, H. V., Zasloff, M., Rosner, J. L., Hendler, R. W., De Waal, A., Vaz Gomes, A., Jongsma, P. M., Riethorst, A., and Juretic, D. (1995) *Eur. J. Biochem. 228*, 257−264.
16. Böttcher, C. J. F., van Gent, C. M., and Pries, C. (1961) *Anal. Chim. Acta 24*, 203−204.
17. Wiseman, T., Williston, S., Brandts, J. F., and Lin, L. N. (1989) *Anal. Biochem. 179*, 131−137.
18. Chen, Y. H., Yang, J. T., and Martinez, H. M. (1972) *Biochemistry 11*, 4120−4131.
19. Seelig, J., and Waespe-Sarcevic, N. (1978) *Biochemistry 17*, 3310−3315.
20. Tamm, L. K., and Seelig, J. (1983) *Biochemistry 22*, 1474−1483.
21. Seelig, J. (1997) *Biochim. Biophys. Acta 1331*, 103−116.

22. Wenk, M. R., and Seelig, J. (1998) *Biochemistry 37*, 3909−3916.
23. Seelig, J., Nebel, S., Ganz, P., and Bruns, C. (1993) *Biochemistry 32*, 9714−9721.
24. Wieprecht, T., Beyermann, M., and Seelig, J. (1999) *Biochemistry 38*, 10377−10387.
25. McLaughlin, S. (1977) *Curr. Top. Membr. Transp. 9*, 71−144.
26. McLaughlin, S. (1989) *Annu. Rev. Biophys. Biophys. Chem. 18*, 113−136.
27. Aveyard, R., and Haydon, D. A. (1973) *An introduction to the principles of surface chemistry*, Cambridge University Press, London.
28. Seelig, J. (1977) *Q. Rev. Biophys. 10*, 353−418.
29. Scherer, P. G., and Seelig, J. (1989) *Biochemistry 28*, 7720−7728.
30. Seelig, J., Macdonald, P. M., and Scherer, P. G. (1987) *Biochemistry 26*, 7535−7541.
31. Seelig, J., and Ganz, P. (1991) *Biochemistry 30*, 9354−9359.
32. Tanford, F. (1980) *The hydrophobic effect: formation of micelles and biological membranes*, Wiley & Sons, New York.
33. Wieprecht, T., Apostolov, O., Beyermann, M., and Seelig, J. (1999) *J. Mol. Biol. 294*, 785−794.
34. Privalov, P. L., and Gill, S. J. (1988) *Adv. Protein Chem. 39*, 191−234.
35. Wenk, M. R., Alt, T., Seelig, A., and Seelig, J. (1997) *Biophys. J. 72*, 1719−1731.
36. Rowe, E. S., Zhang, F., Leung, T. W., Parr, J. S., and Guy, P. T. (1998) *Biochemistry 37*, 2430−2440.
37. Büldt, G., Gally, H. U., Seelig, J., and Zaccai, G. (1979) *J. Mol. Biol. 134*, 673−691.
38. Seelig, J., Gally, G. U., and Wohlgemuth, R. (1977) *Biochim. Biophys. Acta 467*, 109−119.
39. Beschiaschvili, G., and Seelig, J. (1991) *Biochim. Biophys. Acta 1061*, 78−84.
40. Kuchinka, E., and Seelig, J. (1989) *Biochemistry 28*, 4216−4221.
41. Dathe, M., Schümann, M., Wieprecht, T., Winkler, A., Beyermann, M., Krause, E., Matsuzaki, K., Murase, O., and Bienert, M. (1996) *Biochemistry 35*, 12612−12622.
42. Wieprecht, T., Dathe, M., Epand, R. M., Beyermann, M., Krause, E., Maloy, W. L., MacDonald, D. L., and Bienert, M. (1997) *Biochemistry 36*, 12869−12880.

BI992146K